International Journal of Heat and Mass Transfer 51 (2008) 6039–6046

Contents lists available at ScienceDirect

International Journal of Heat and Mass Transfer

journal homepage: www.elsevier.com/locate/ijhmt

Characterization of evaporator and condenser thermal resistances of a screen mesh wicked heat pipe

R. Kempers [a], A.J. Robinson [b], D. Ewing [a,1], C.Y. Ching [a,*]

[a] Department of Mechanical Engineering, McMaster University, Hamilton, Ontario, Canada L8S 4L7
[b] Department of Mechanical and Manufacturing Engineering, Trinity College Dublin, Ireland

ARTICLE INFO

Article history:
Received 24 September 2007
Received in revised form 22 March 2008
Available online 14 May 2008

Keywords:
Wicked heat pipe
Evaporator
Boiling heat transfer
Composite heat transfer model

ABSTRACT

The heat transfer mechanisms in the condenser and evaporator sections of a copper-water wicked heat pipe with 3 layers of screen mesh were investigated experimentally. The individual condenser and evaporator thermal resistances were measured using thermocouples on the outer wall and within the core of the heat pipe. The heat transfer in the condenser section was found to be only by conduction. In the evaporator, however, either conduction or boiling heat transfer can occur. The transition between the two modes was found to be dependent on the vapor pressure and heat flux, and was reasonably well predicted by the bubble nucleation criterion outlined by Van Stralen and Cole [S. Van Stralen, R. Cole, Boiling Phenomena, vol. 1, McGraw-Hill Inc., 1979]. The experimental data for the boiling heat transfer in the evaporator was well correlated by $[St][Pr]^{0.6}[N_p]^{0.2} = 0.13[Re]^{-1.43}$. A composite heat transfer model for the heat pipe is proposed that considers both conduction and boiling heat transfer in the evaporator.

1. Introduction

There has been renewed interest in the use of heat pipes for thermal management due to increasing heat flux requirements and thermal constraints in many industrial applications. The performance of heat pipes is characterized both by the effective thermal resistance and the maximum heat transport capacity. The maximum heat transport in moderate temperature applications is limited by the capillary pressure that can be generated by the wick structure [1]. Thus, several models have been developed to predict the pressure drop that occurs in wicked heat pipes [1–3]. The effective thermal resistance that determines the heat transfer rate for a given set of boundary conditions is often modelled using a thermal resistance network [4,5], where each component of the heat pipe is modelled by an associated thermal resistance. The resistance to heat transfer across the saturated wick structure at the condenser and evaporator represents the dominant thermal resistances in this network [4–6]. The simplest models ignore axial conduction along the heat pipe and vapour (appropriate for moderate temperature applications), while other models have been developed that consider the heat transfer along the wall and the thermal resistance of the vapour region [7,8].

The heat transfer in the liquid saturated wick is commonly modelled as conduction across it with condensation and evaporation at the free surface [4–6]. A number of empirical, semi-empirical and analytical models have been developed for the effective thermal conductivity of saturated screen mesh wicks [4–6]. The predictions of these models, however, can vary by several orders of magnitude for the same wick-working fluid combination [9]. A number of investigations have shown that the heat transfer in the condenser section does appear to be conduction, and most models assume the same is true in the evaporator [1,4–6]. Ambrose et al. [10] noted, however, that a conduction model may not be appropriate for the evaporator. They argued that boiling would likely occur in the wick, due in part to the large temperature drop across the wick and the large number of favourable nucleation sites present in a porous structure. Semena [11] suggested that, for metal fibre wicks, the heat is conducted across the saturated wick with evaporation at the free surface for heat fluxes below 10 kW/m^2, but for heat fluxes above this the heat transfer mechanism transitions to boiling. In the early work on heat pipes, Marto and Mosteller [12] visually observed the onset of boiling in an inverted heat pipe enclosed in a glass container for heat fluxes between 10 and 15 kW/m^2.

Allingham and McEntire [13] proposed that the boiling in a saturated ceramic wick at various pressures could be modelled by modifying a correlation to characterize boiling on a copper surface as [14]

$$[St]^a[Pr]^b[N_p]^c = d[Re]^e \quad (1)$$

that included both pressure and surface tension effects in N_p, the pressure number. The flow rate effect in the Stanton number and

* Corresponding author. Tel.: +1 905 525 9140x24998; fax: +1 905 572 7944.
E-mail address: chingcy@mcmaster.ca (C.Y. Ching).
[1] Current Address: Department of Mechanical and Materials Engineering, Queen's University, Ontario, Canada.

0017-9310/$ - see front matter © 2008 Elsevier Ltd. All rights reserved.
doi:10.1016/j.ijheatmasstransfer.2008.04.001

Nomenclature

A	area, m^2
C_p	specific heat, kJ/kg K
d	diameter, m
D	characteristic dimension, m
f	friction factor
G	mass velocity, kg/m^2 s
g	gravitational constant, m/s^2
h	heat transfer coefficient, W/m^2 K
h_{fg}	enthalpy of evaporation, J/kg
I	current, A
K	permeability, m^2
k	conductivity, W/m K
L	length, m
N_p	pressure number, $\left[\frac{g\rho_l\sigma}{P^2}\right]$
P	absolute pressure, Pa
Pr	Prandtl number, $\left[\frac{C_p\mu_l}{k_l}\right]$
Q	heat transfer rate, W
q''	heat flux, W/m^2
R	universal gas constant, J/mol K
Re	Reynolds number, $\left[\frac{DG}{\mu_l}\right]$
r	radius, m
r_c	radius of nucleation site, m
St	Stanton number, $\left[\frac{h}{C_pG}\right]$
T	temperature, °C
V	voltage, V

Greek symbols

δ	wick thickness, m
ε	porosity
μ	viscosity, Ns/m^2
ρ	density, kg/m^2
σ	surface tension, N/m

Subscripts

a	active
c	condenser
e	evaporator
g	non-condensable gas
h	hydraulic
i	inner
l	liquid
o	outer
v	vapour
w	wall

Reynolds number was characterized by the mass flow rate through the wick.

There have been some direct measurements in the vapour core of wicked heat pipes under steady state operation. El-Genk and Huang [15] measured the vapour temperature distribution of a copper-water heat pipe during transient operation, but presented data for only a single steady-state case. Anand [16] measured the vapour temperature of a stainless steel heat pipe with a stainless steel screen mesh wick to characterize the boiling heat transfer in the evaporator section and found the heat transfer could be correlated using Eq. (1). A number of studies have also presented evaporator heat transfer coefficient data, summarized by Chisholm et al. [17] that indicate the effective conductivity of the wick is not uniform.

Despite the evidence of boiling in the evaporator section, most numerical models tend to ignore this phenomenon when characterizing the performance of heat pipes. Thus the objective of the current investigation was to characterize the individual condenser and evaporator thermal resistances of a copper-water screen mesh wicked heat pipe to examine again if there is boiling heat transfer in the heat pipe and to consider the importance of considering this heat transfer mechanism when modelling the performance of the heat pipe. In particular, the heat transfer mechanisms in the heat pipe were investigated by simultaneously measuring the axial wall and vapour temperature distributions for different operating pressures. The experiments were performed using a custom-built heat pipe that was instrumented with thermocouples within the core and along the wall of the heat pipe. This allowed for a quantitative determination of the individual component thermal resistances of the heat pipe. The experimental facilities are described in the next section, followed by a discussion of the results and the conclusions from this study.

2. Experimental facilities

The experiments were performed using a 19.05 mm outer-diameter copper-water heat pipe with a length of 355.6 mm and a wall thickness of 1.65 mm. The wick consisted of 3 wraps of a copper wire screen mesh with a wire diameter of 0.11 mm and 3937 strands per meter. The heat pipe was charged with 7.13 mL of water, which approximately corresponds to the amount required to completely saturate the wick based on a standard model for screen mesh porosity [18]. The wall temperature distribution of the heat pipe was measured using eleven evenly spaced 0.51 mm T-type thermocouples with an uncertainty of ±0.5 °C, shown schematically in Fig. 1, with the distance of the thermocouples from the evaporator end given below each location. The thermocouples were embedded along 0.58 mm by 0.76 mm grooves that were machined on the outer surface of the wall. The internal vapour temperature distribution was measured using four evenly spaced 0.51 mm K-type thermocouples with an uncertainty of ±1.1 °C that were inserted through holes drilled through the heat pipe wall and wick prior to charging. In this case, the thermocouple junctions were positioned along the centreline and the leads were silver soldered in place along the machined grooves.

The evaporator section of the heat pipe was clamped between two halves of an 88.9 mm diameter aluminium annulus that was 101.6 mm long. The annulus was heated on the outside using two 50.8 mm wide 750 W electric band heaters. Thermally conductive paste was used to reduce the contact resistance between the heat pipe, annulus and band heaters. The electrical power to the band heaters was supplied using a 220 V variable AC power supply and measured using a power transducer with uncertainty ±2.5 W. The entire evaporator section was clamped between two halves of a wooden block lined with 25.4 mm of ceramic insulation to prevent heat loss to the ambient. The condenser section of the heat pipe was cooled using water flow through a 152.4 mm long acrylic jacket with an inner diameter of 25.4 mm. The cooling water entered and exited the jacket through eight 11.13 mm diameter ports equally spaced around the circumference that were 12.7 mm from the ends of the condenser section. Headers feeding the inlet and outlet ports were used to ensure a relatively even flow rate through the ports. The cooling water was supplied either from a dedicated chiller or from a heated water loop with the water temperature controlled using a thermocouple and a PID controller. The water flow rate was measured using a dual-rotor turbine flow me-

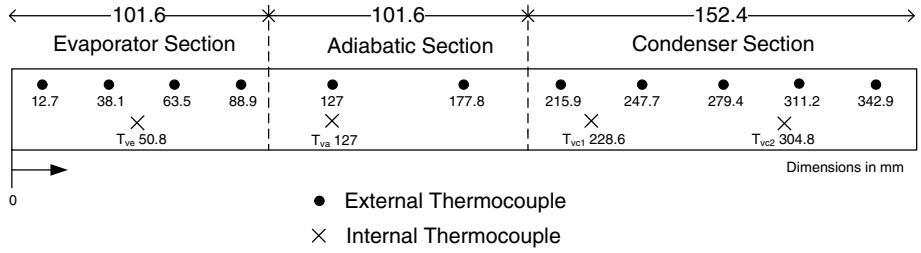

Fig. 1. Schematic of instrumented heat pipe showing locations of thermocouples.

ter on the inlet line to the acrylic jacket that had an uncertainty of ±0.1%. The inlet and outlet temperatures of the cooling water were measured using two 4-wire platinum RTDs with uncertainties of ±0.014 °C. All fittings and header components were plastic and wrapped in foam insulation to minimize heat transfer with the ambient. The data from the thermocouples, RTD thermometers, turbine flow meter, and power transducer were acquired at a sampling frequency of 1 Hz. The output heat transfer rate from the condenser was computed by applying an energy balance to the condenser flow. The effect of heat losses to the ambient and viscous heating effects were characterized independently, and subtracted from the output heat transfer rate. In all cases, the heat transfer rate into the evaporator section and out of the condenser section agreed to within ±5%, which was within the experimental uncertainty associated with each respective heat transfer measurement. The uncertainties of the calculated quantities are summarized in Table 1.

The experiments were performed with the heat pipe in the horizontal orientation. In the first series of tests, the heat input to the evaporator was increased in steps of 10–15 W while the mean condenser wall temperature was maintained constant using the chilled water supply. Tests were performed for condenser wall temperatures of 12, 20 and 35 °C. In the second series of tests, the evaporator heat input was increased while holding the vapour temperature constant by adjusting the temperature of the water to the condenser jacket from the heated water loop. In these tests, the output of the thermocouple located in the adiabatic section of the heat pipes was used as the input to the PID controller of the heated water loop. The tests were performed for vapour temperatures of 50, 70 and 80 °C. For all tests, the heat pipe was allowed to reach steady state and the data was recorded over a time interval of 60 s.

3. Results and discussion

The external wall temperature distributions for the test with a constant condenser wall temperature of 20 °C at different heat inputs are shown in Fig. 2. As expected, the evaporator wall temperature increases with input power and remains relatively isothermal. At the higher heat transfer rates, however, the temperature from the end most thermocouple towards the evaporator end cap is lower than the rest of the evaporator, the reason of which is not clear. There is a temperature gradient within the adiabatic section, which becomes more significant at higher heat transfer, indicating some axial heat conduction along the wall. The heat transfer along the wall estimated from the temperature gradient in the adiabatic section was less than 2% of the total heat transfer. The internal axial temperature distributions corresponding to Fig. 2 are shown in Fig. 3. The core temperature in the evaporator and adiabatic sections are nearly equal and increase with the heat input as expected. The core temperature in the condenser section is close

Table 1
Uncertainties of the calculated quantities

Quantity	Equation	Uncertainty
Electrical power	$Q_{elec} = IV$	±1.8%
Mean evaporator temperature	$T_e = \frac{T_1 + T_2 + T_3 + T_4}{4}$	±1 °C
Mean condenser temperature	$T_c = \frac{T_5 + T_6 + T_7 + T_8}{4}$	±1 °C
Evaporator and condenser temperature difference	$T_e - T_c$	±1.4 °C
Effective thermal resistance	$R_{eff} = \frac{T_e - T_c}{Q_{evap}}$	±20% for $Q < 10$ W ±10% for $10 < Q < 30$ W ±5% for $Q > 30$ W
Effective thermal conductivity	$k_{eff} = \frac{\ln\left(\frac{r_o}{r_i}\right)}{2\pi R_{eff} L}$	±20% for $Q < 10$ W ±10% for $10 < Q < 30$ W ±5% for $Q > 30$ W
Heat transfer coefficient	$h = \frac{q''_e}{T_{e,w} - T_v}$	±22% for $Q < 10$ W ±11% for $10 < Q < 30$ W ±6% for $Q > 30$ W

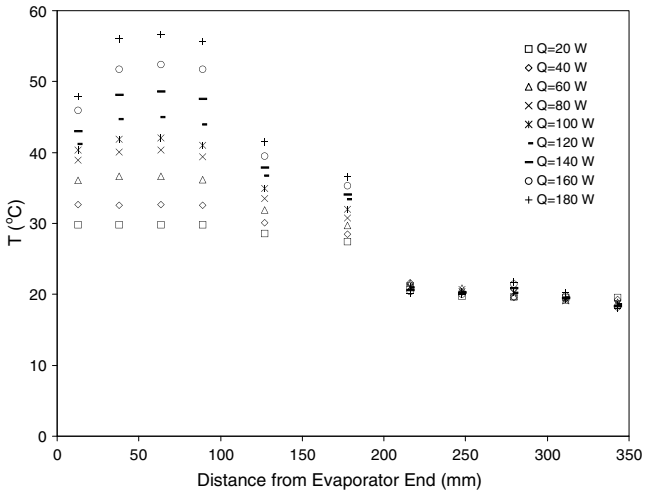

Fig. 2. Axial variation of wall temperature with heat input for a constant condenser wall temperature of 20 °C.

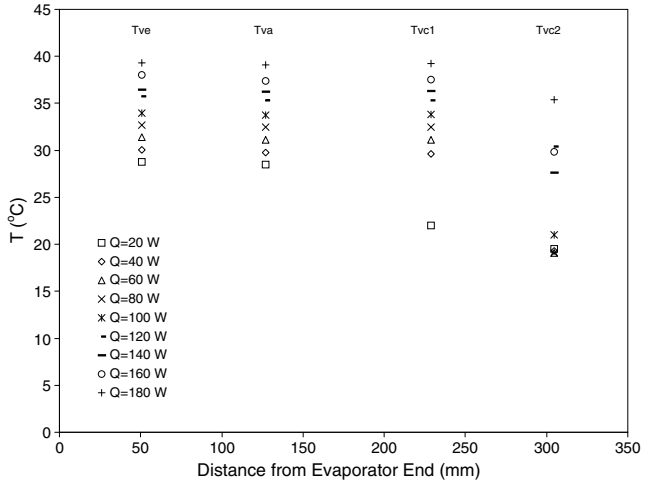

Fig. 3. Axial variation of internal core temperature with heat input for a constant condenser wall temperature of 20 °C.

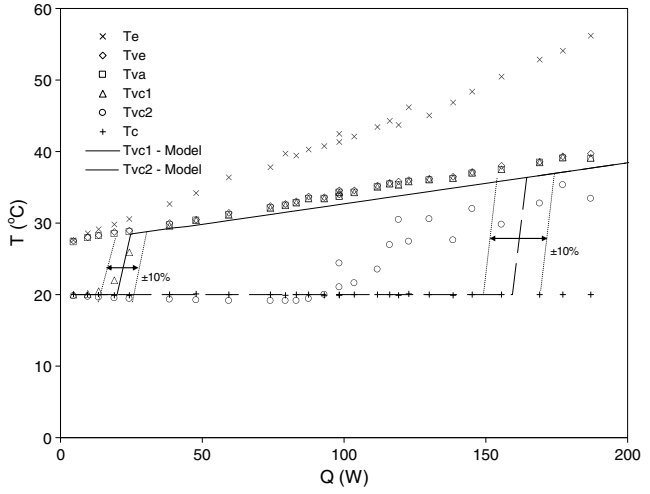

Fig. 4. Variation of wall and core temperatures with heat input for a constant condenser wall temperature of 20 °C.

to that of the condenser wall at the lowest heat input of 20 W, and significantly lower than that in the evaporator and adiabatic sections. The core temperature closer to the adiabatic section (T_{vc1}) increases for heat inputs above 40 W and approaches that in the adiabatic and evaporator sections. The core temperature closer to the condenser end cap (T_{vc2}) subsequently increases at a higher heat flux, indicating that a greater region of the condenser becomes effective as the heat flux is increased.

This is further illustrated in Fig. 4 where the internal temperature measurements are plotted as a function of the heat transfer rate. The mean evaporator and condenser wall temperatures are also shown in this figure. The mean evaporator wall temperature reported here was estimated using all the data points, including that from the end most thermocouple that showed a lower temperature from the rest of the evaporator. Excluding this data point in computing the mean, however, did not significantly change any results or the interpretation therein. The core temperature in the evaporator and adiabatic sections are approximately equal and increases with the heat input as shown previously in Fig. 3. Within the condenser section, the core temperature towards the adiabatic section is initially at the condenser wall temperature, and increases sharply to that in the adiabatic section as the heat input reaches approximately 20 W. The increase in the core temperature towards the condenser end cap occurs at a much higher heat input of approximately 120 W, and the increase in this case is not as sharp as before. The data is consistent with the presence of non-condensable gases (NCG) that tend to accumulate at the condenser end of the heat pipe. At low heat fluxes, the non-condensable gases occupy a larger portion of the condenser due to the lower vapour pressure, resulting in the core temperature of this region being close to the condenser wall temperature. As the heat flux increases, the operating (vapour) temperature of the heat pipe increases, increasing the vapour pressure which compresses the non-condensable gases and thereby increasing the active region of the condenser.

The effective thermal conductivity of the condenser and evaporator sections was determined directly from the wall and core temperature measurements. For the condenser section, only the active length of the condenser, $L_{c,a}$, was considered when evaluating the effective thermal conductivity, k_c. The result is

$$k_c = \frac{\ln\left(\frac{r_o}{r_i}\right)}{2\pi R_c L_{c,a}}, \tag{2}$$

where the thermal resistance of the condenser is given by

$$R_c = \frac{T_v - T_{c,w}}{Q}. \tag{3}$$

The active length of the condenser was estimated using a simple flat front model for the non-condensable gases that neglects vapour-gas diffusion or inertial effects of the vapour flow. The active length in this case is given by [4]

$$L_{c,a} = L_c - \frac{m_g R_g T_c}{(P_{v,a} - P_{v,c})A_v}, \tag{4}$$

where L_c is the overall length of the condenser, m_g and R_g are the mass and gas constant of the non-condensable gases, and A_v is the cross-sectional area of the vapour core. This model requires the knowledge of the mass and species of the non-condensable gases *a priori*. It was assumed the non-condensable gas was air, and the mass was estimated by varying the m_g until the location of the front matched that observed in the core temperature measurements for different operating conditions. A mass of 3.65×10^{-7} kg fit the experimental data reasonably well in this case as shown in Fig. 4, where the model predictions for T_{vc1} and T_{vc2} are compared to the experimental data. The core temperature measurements towards the condenser end cap (T_{vc2}), however, show that

diffusion and flow effects become significant as the vapour front moves towards the condenser end with an increase in heat flux. The relatively large amount of non-condensable gases seemed associated with the internal instrumentation. Tests with heat pipes without this instrumentation contained considerably less non-condensable gases.

The variation of the condenser thermal conductivity with the evaporator heat flux at different fixed condenser temperatures is shown in Fig. 5. The thermal conductivity of the condenser remains relatively constant and is reasonably well estimated by the model of Chang [19] for the effective conductivity of a water saturated wire screen mesh. This suggests that the heat transfer across the wick at the condenser section is well modelled by conduction.

The effective thermal conductivity of the evaporator section is plotted as a function of the heat flux in Fig. 6 for the different fixed condenser and vapour temperatures. For the cases with the fixed condenser wall temperatures (and lower vapour temperatures), the conductivity is approximately constant and in reasonable agreement with the conduction model of Chang [19]. For cases with the fixed higher vapour temperature, however, the thermal conductivity at heat fluxes below 15 kW/m^2 is significantly higher than could be explained by conduction heat transfer. Previous investigations suggest that conduction was the dominant mechanism at the lower heat fluxes and boiling was the primary mechanism for heat transfer in the evaporator above approximately 10–15 kW/m^2 [11,12]. The present data indicates this is not the case for the higher vapour temperature.

The thermal resistance of the evaporator can also be expressed in terms of a heat transfer coefficient given by

$$h = \frac{q''_e}{T_{e,w} - T_v} \tag{5}$$

The change in heat transfer coefficient with temperature difference between the evaporator wall and vapour are shown in Fig. 7, along with the values predicted by the conduction models of Semena [11] and Chang [19], an experimental correlation from Kunz et al. [20] for a 7 layer screen mesh wick, and a boiling heat transfer correlation developed by Anand [16]. This figure clearly shows that conduction occurs only at the lower superheats for the lower operating temperature cases, denoted by the open symbols. At the higher superheats, denoted by the black-filled symbols, the heat transfer is boiling, with the grey-filled symbols showing the transition from conduction to boiling heat transfer in the evaporator. For the higher operating temperature cases, there is only boiling heat transfer in the evaporator. The data for the boiling heat transfer show the same trend as the correlation by Anand [16], but with higher values.

Van Stralen and Cole [21] proposed that for a uniform temperature system the liquid superheat required to initiate bubble nucleation can be approximated by the expression

$$T_w - T_{sat}(P_l) = \frac{2\sigma T_{sat}(P_l)}{\rho_v h_{fg} r_c}, \tag{6}$$

where r_c is the nucleation site radius. As a first approximation, the liquid temperature can be assumed to be at the evaporator wall temperature here. For the case when there is a linear temperature gradient between the wall and the inner surface of the wick, the Griffith [22] nucleation criteria can be used, which simplifies to

$$T_w - T_{sat}(P_l) = \frac{2\sigma T_{sat}(P_l)}{\rho_v h_{fg} r_c}\left(\frac{1}{1-(r_c/\delta)}\right), \tag{7}$$

where, for this analysis, δ is taken as the wick thickness and the temperature at the vapour–liquid interface at the wick inner surface is assumed to be at the saturation temperature. In both cases, the correlations indicate that the superheat necessary to initiate boiling depends on the vapor pressure (or temperature) and the fluid temperature as was observed.

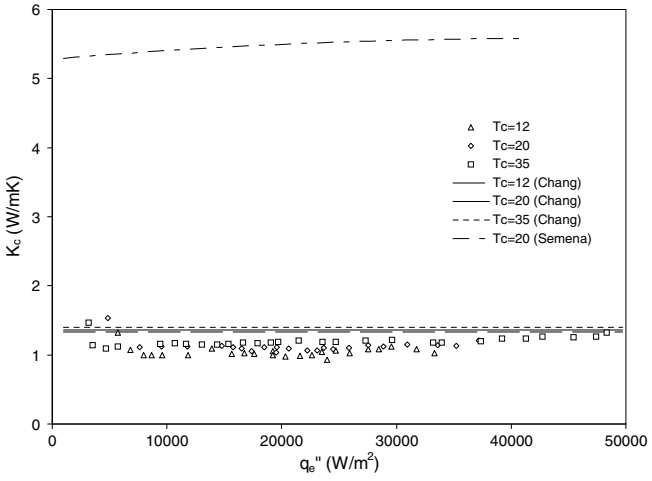

Fig. 5. Change in condenser conductivity with heat flux for different condenser wall temperatures.

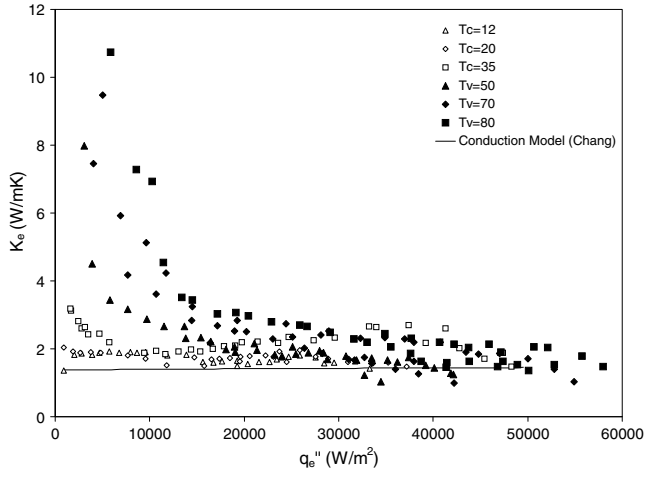

Fig. 6. Change in evaporator conductivity with heat flux.

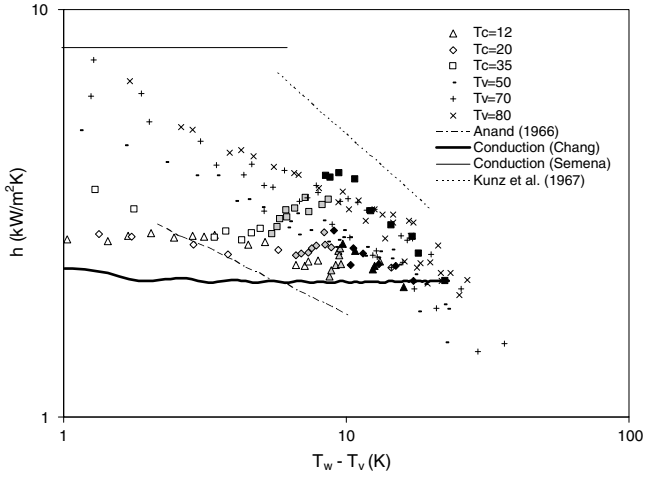

Fig. 7. Change in evaporator heat transfer coefficient with wall superheat. The open symbols indicate conduction, grey-filled symbols indicate transition and black-filled symbols indicate boiling for the constant wall temperature data.

It is well established that the onset of boiling occurs at a much lower wall superheat for surfaces in contact with a porous media compared to a bare surface due to more favourable nucleation sites for the initiation of bubble activity [23]. The size of the nucleation sites near the wall is difficult to estimate for wire mesh heat pipes because it will depend on how well the mesh sits on the wall. The superheat necessary for bubble nucleation was estimated here using the effective pore radius of the wick as the critical nucleation site radius so that $r_c = 0.127$ mm, which is likely smaller than the sites near the wall. The estimate of the superheat, plotted in Fig. 8 for the operating pressures and temperatures considered here, show an inverse relationship between the required nucleation superheat and system pressure. Little superheat is required to initiate boiling at high system pressures. At low system pressures, the superheat required to initiate boiling, however, increases very rapidly with decreasing pressure. The current data is also shown in Fig. 8, and is consistent with the bubble nucleation criterion, but does not exactly match the transition curve. This is likely due to the difficulty in estimating the radius of nucleation sites at the interface between the mesh screen and the wall of the heat pipe.

The data with boiling heat transfer are presented in the non-dimensional form $[St][Pr]^a[N_p]^b = C[Re]^c$ suggested by Anand [16] in Fig. 9. The mass velocity here is given by

$$G = \frac{Q}{A_w \varepsilon h_{fg}} \tag{8}$$

and the characteristic dimension for the Reynolds number is taken as

$$D = 4r_h \tag{9}$$

where r_h is the hydraulic diameter of the wick. For liquid saturated screen meshes, it is difficult to determine the hydraulic radius analytically. The hydraulic radius was determined by equating the definition of wick permeability [4],

$$K = \frac{2\varepsilon r_h^2}{(fRe)} \tag{10}$$

to a correlation developed by Marcus [18] for screen mesh wicks

$$K = \frac{d^2\varepsilon^3}{122(1-\varepsilon)^2} \tag{11}$$

where d is the wire diameter, ε is the wick porosity and $(fRe) = 64$ assuming laminar flow. The hydraulic radius is thus given by

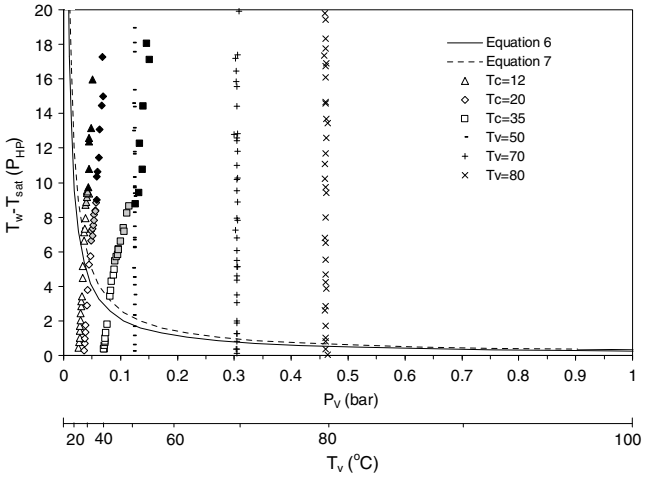

Fig. 8. Variation of wall superheat with heat pipe operating pressure showing the regions of expected nucleate boiling within the wick (above analytic curves) and expected conduction across the wick (below analytic curves).

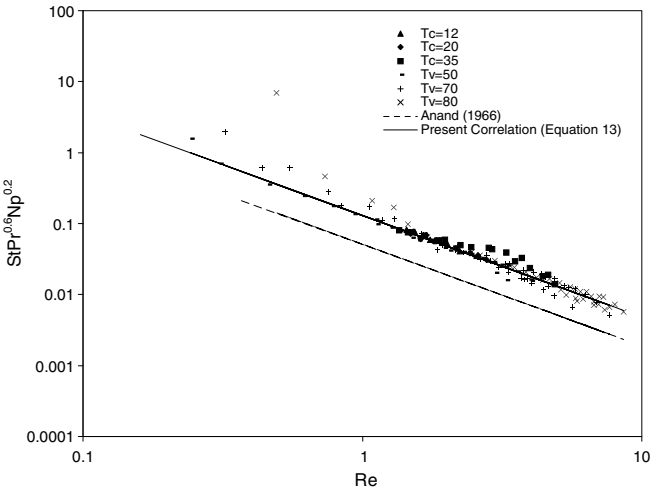

Fig. 9. Boiling heat transfer correlation for the evaporator screen mesh wick.

$$r_h = \sqrt{\frac{16d^2\varepsilon^2}{61(1-\varepsilon)^2}} \tag{12}$$

The results show that the boiling heat transfer data at the different operating temperatures collapse to a line that has the same slope to the correlation proposed by Anand [16], but with higher values. The present data for the boiling heat transfer in the evaporator is well correlated by

$$[St][Pr]^{0.6}[N_p]^{0.2} = 0.13[Re]^{-1.43}. \tag{13}$$

4. Composite heat pipe heat transfer model

The heat transfer mechanism in the evaporator is conduction at relatively low vapour temperatures and low evaporator heat fluxes, and boiling otherwise. Hence, it indicates a composite heat transfer model should be used to predict the performance of the evaporator section in wicked heat pipes that considers either conduction or boiling. The transition between the two modes could be estimated using a nucleation criterion such as those proposed in Eqs. (6) and (7). The results here show that this does not exactly predict the transition point, so a more sophisticated model may be necessary to refine the criteria, particularly if the operating region is close to the transition zone. The effective conductivity for the conduction mode can be determined from a model such as Chang's [19], while the heat transfer in the boiling mode can be determined using a correlation such as Eq. (13). The heat transfer in the condenser section would be modelled by a conduction model such as Chang's [19], with a model for the non-condensable gases as necessary.

The predictions from the composite model for the constant condenser wall temperature cases are compared to the measurements in Fig. 10. There is very little heat transfer at small temperature differences when the condenser temperature is low, and this offset "turn-on" temperature difference reduces as the condenser temperature is increased. This was not captured when the effect of the non-condensable gases was omitted, but was reasonably well predicted with the inclusion of the flat front model for the non-condensable gases as seen in Fig. 10. Thus, this offset temperature difference is caused by the non-condensable gases. The composite model captures the transition in the evaporator heat transfer from conduction to boiling reasonably well. The sudden jog in the curve at the transition between the conduction and boiling modes is due to the sharp demarcation assumed in the composite model between the two modes. To better capture the transition zone, a more

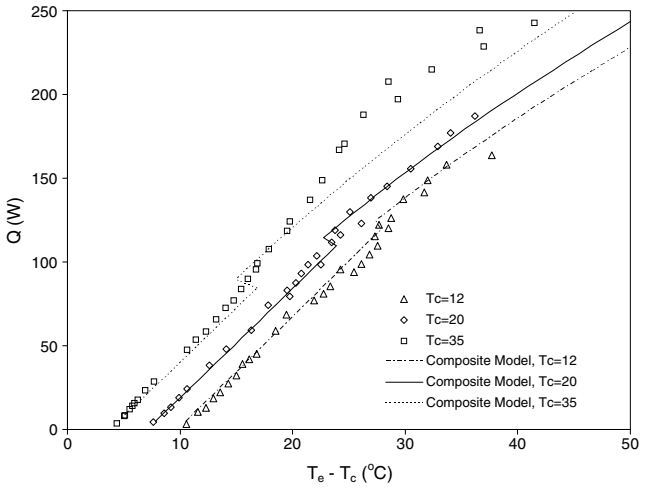

Fig. 10. Change in heat transfer rate with temperature difference for different condenser wall temperatures.

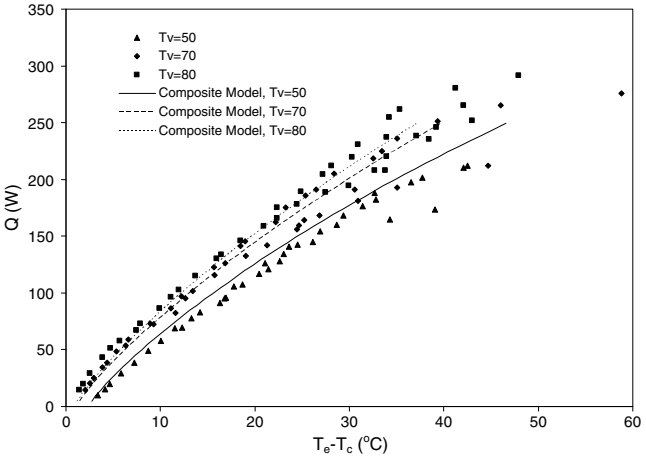

Fig. 11. Change in heat transfer rate with temperature difference for different vapour temperatures.

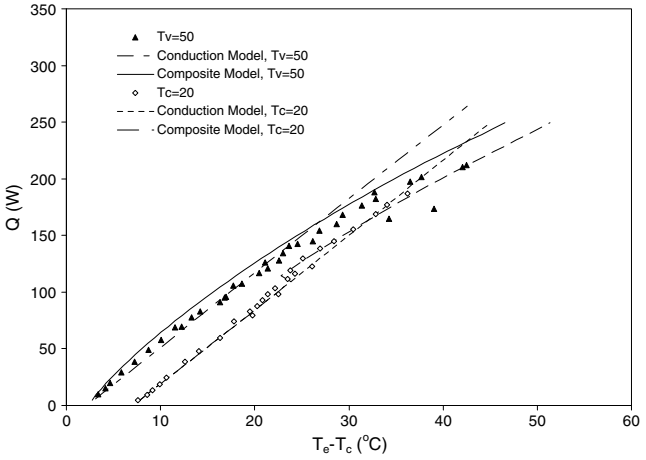

Fig. 12. Comparison between conduction only model and proposed composite model.

sophisticated model in this region that blends the two modes may be necessary. The composite model predictions are compared to the data for the constant vapour temperature tests in Fig. 11. Here, the heat transfer in the evaporator was boiling for all conditions, and hence the jog showing the transition from conduction to boiling heat transfer is not present. The composite model is able to capture the non-linearity in the data in this region reasonably well.

The predictions from the model that considers conduction only in both the condenser and evaporator and the present composite model are shown in Fig. 12. It is clear that the conduction only model can not capture the non-linearity of the data nor the transition as the heat transfer mode changes from conduction to boiling in the evaporator. As expected, the conduction only model deviates significantly from the experimental data when there is boiling heat transfer in the evaporator.

5. Conclusions

The heat transfer in the evaporator and condenser sections of a copper-water wicked heat pipe with a three-layer copper screen mesh wick was characterized by measuring the internal and wall temperature distributions under different operating conditions. The effective thermal conductivity of the saturated wick in the condenser section based on the active length of the condenser was well predicted by the conduction model of Chang [19], indicating that conduction is the dominant mode of heat transfer across the saturated wick in the condenser. In the evaporator, either conduction or boiling heat transfer can take place. The mode of heat transfer is dependent on the vapour pressure and heat flux, with boiling occurring even for very low heat fluxes or superheat for operating temperatures above 50 °C. The onset of boiling in the evaporator could be reasonably predicted using a bubble nucleation criterion [21,22]. The boiling heat transfer in the evaporator was well characterized by a boiling heat transfer correlation of the form $[St][Pr]^{0.6}[N_p]^{0.2} = 0.13[Re]^{-1.43}$, which is similar to other correlations for nucleate boiling heat transfer [8–10].

Thus, the results show that a composite heat transfer model should be used for wicked heat pipes that takes into account that either conduction or boiling can occur in the evaporator, with conduction only at the condenser. The transition between the conduction and boiling in the evaporator can be estimated using a bubble nucleation criteria [21]. The predictions from this composite model, using the boiling correlation proposed in this study, were in good agreement with the experimental data.

Acknowledgements

The support of the Natural Sciences and Engineering Research Council (NSERC) of Canada, Ontario Centres of Excellence (OCE), Acrolab Ltd. and Long Manufacturing – Thermal Products Division of Dana Corporation is gratefully acknowledged.

References

[1] A. Faghri, Heat Pipe Science and Technology, Taylor and Francis, Washington, DC, 1995.
[2] N. Zhu, K. Vafai, Analysis of cylindrical heat pipes incorporating the effects of liquid-vapor coupling and non-Darcian transport – a closed form solution, Int. J. Heat Mass Transfer 42 (1999) 3405–3418.
[3] K.A.R. Ismail, M.A. Zanardi, A steady-state model for heat pipes of circular or rectangular cross sections, J. Appl. Therm. Eng. 16 (1996) 753–767.
[4] S.W. Chi, Heat Pipe Theory and Practice, McGraw-Hill, New York, 1976.
[5] G.P. Peterson, An Introduction to Heat Pipes: Modeling, Testing, and Applications, John Wiley, New York, 1994.
[6] P.D. Dunn, D.A. Reay, Heat Pipes, second ed., Pergamon Press, Oxford, England, 1978.
[7] K.H. Sun, C.L. Tien, Thermal performance characteristics of heat pipes, Int. J. Heat Mass Transfer 18 (1975) 363–380.

[8] J.M. Tournier, M.S. El-Genk, Heat pipe transient analysis model, Int. J. Heat Mass Transfer 37 (1994) 753–762.
[9] R. Kempers, C.Y. Ching, D. Ewing, Effect of number of mesh layers and fluid loading on the performance of screen mesh wicked heat pipes, J. Appl. Therm. Eng. 26 (2006) 589–595.
[10] J.H. Ambrose, R. Ponnappan, J.E. Beam, E.T. Mahefkey, A boiling heat transfer correlation for heat pipes, Society of Automotive Engineers, in: 15th Intersociety Conference on Environmental Systems, San Francisco, California, 1985 (SAE Paper 851326).
[11] M.G. Semena, Method of computing the thermal resistance of low-temperature heat pipes with metal-fiber wicks, J. Eng. Phys. 36 (1979) 287–292.
[12] P.J. Marto, W.L. Mosteller, Effect of nucleate boiling on the operation of low temperature heat pipes, ASME Paper 69-HT-24, American Society of Mechanical Engineers, 1969.
[13] W.D. Allingham, J.A. McEntire, Determination of boiling film coefficient for a heated horizontal tube in water-saturated wick material, J. Heat Transfer 83 (1961) 71–76.
[14] C.H. Gilmour, Nucleate boiling – a correlation, Chem. Eng. Prog. 54 (1958) 77–79.
[15] M.S. El-Genk, L. Huang, Experimental investigation of the transient response of a water heat pipe, Int. J. Heat Mass Transfer 36 (1993) 3823–3830.
[16] D.K. Anand, On the performance of a heat pipe, J. Spacecraft Rockets 3 (1966) 763–765.
[17] D. Chisholm, The Heat Pipe, Mills and Boon, London, 1971.
[18] B.D. Marcus, Theory and design of variable conductance heat pipes, NASA CR-2018, 1972.
[19] W.S. Chang, Porosity and effective thermal conductivity of wire screens, J. Heat Transfer 112 (1990) 5–9.
[20] H.R. Kunz, L.S. Langson, B.H. Hildton, Vapour-chamber fin studies. Transport properties and boiling characteristics of wicks, NASA CR-812, 1967.
[21] S. Van Stralen, R. Cole, Boiling Phenomena, vol. 1, McGraw-Hill Inc., 1979.
[22] P. Griffith, Nucleation and bubble formation in boiling, Proceedings of the Institution of Mechanical Engineers 180 (Pt 1) (1965–1966) 1092–1098.
[23] A. Abhat, R.A. Seban, Boiling and evaporation from heat pipe wicks with water and acetone, J. Heat Transfer 96 (1974) 331–337.